

TelePhantom: A User-Friendly Teleoperation System with Virtual Assistance for Enhanced Effectiveness

Jingxiang Guo^{1*}, Jiayu Luo^{1*}, Zhenyu Wei^{1*}, Yiwen Hou¹,
Zhixuan Xu¹, Xiaoyi Lin¹, Chongkai Gao¹, Lin Shao^{1†}



Fig. 1: **TelePhantom** is a user-friendly teleoperation system enabling the real-time virtual preview before robot execution.

Abstract—Dexterous manipulation is a critical area of robotics. In this field, teleoperation faces three key challenges: user-friendliness for novices, safety assurance, and transferability across different platforms. While collecting real robot dexterous manipulation data by teleoperation to train robots has shown impressive results on diverse tasks, due to the morphological differences between human and robot hands, it is not only hard for new users to understand the action mapping but also raises potential safety concerns during operation. To address these limitations, we introduce TelePhantom. This teleoperation system offers real-time visual feedback on robot actions based on human user inputs, with a total hardware cost of less than \$1,000. TelePhantom allows the user to see a virtual robot that represents the outcome of the user’s next movement. By enabling flexible switching between command visualization and actual execution, this system helps new users learn how to demonstrate quickly and safely. We demonstrate its superiority over other teleoperation systems across five tasks, emphasize its ease of use, and highlight its ease of deployment across diverse input sensors and robotic platforms. We will release our code and a deployment document on our website <https://telephantom.github.io/>.

I. INTRODUCTION

Teleoperation has long been recognized as an essential component in gathering on-robot data for learning from demonstrations [1]–[11]. An intuitive and user-friendly teleoperation system is crucial for collecting high-quality, di-

verse, and scalable data. However, effectively controlling robots with dexterous hands remains a significant challenge. The fundamental differences between human and robotic hands make the direct mapping of human movements to robotic actions exceptionally complex. These inherent structural and functional differences, combined with the precision required for precise manipulation tasks, often result in inefficient and potentially compromised data collection processes.

Existing teleoperation systems face three significant challenges. First, novice users often struggle to control the robot effectively due to the lack of intuitive feedback on how their commands translate to robot actions, especially during complex manipulation tasks. Second, without proper safeguards and real-time guidance, users may inadvertently issue unsafe commands that could damage the robot or its surroundings. Third, most current systems are tightly coupled with specific input devices or robot platforms, limiting their adaptability and broader application. These challenges significantly impact the quality and efficiency of data collection for robot learning.

To address these challenges, we introduce TelePhantom, a teleoperation system that delivers precise control while maintaining affordability through its sub-\$1,000 hardware implementation. At its core, TelePhantom provides an interface where a virtual robotic arm spatially overlaps with the physical arm, allowing users to preview and confirm intended movements through an external input device (e.g., a foot pedal) before execution on the physical system.

Building upon this core design, our modular framework (Figure 2) addresses key challenges in human-robot mo-

* denotes equal contribution

† denotes the corresponding author

¹Jingxiang Guo, Jiayu Luo, Zhenyu Wei, Yiwen Hou, Zhixuan Xu, Xiaoyi Lin, Chongkai Gao, and Lin Shao are with the Department of Computer Science, National University of Singapore. jingxiangguo@u.nus.edu, linshao@nus.edu.sg

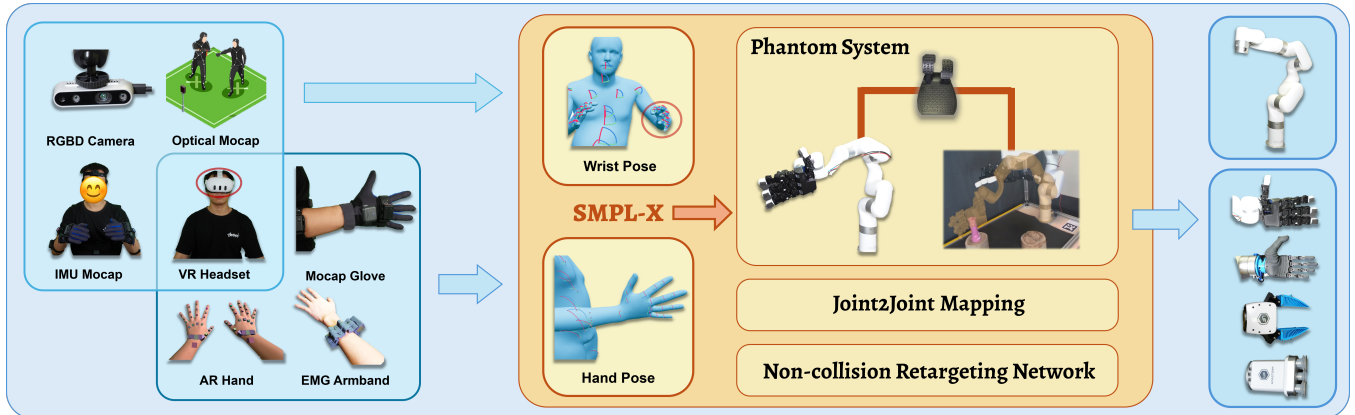


Fig. 2: **Overview of the TelePhantom System Architecture:** Our system consists of three main components: (1) Various input devices including RGBD cameras, IMU mocap suits, VR headsets, mocap gloves, AR hand tracking, and EMG armbands for capturing human motion; (2) A central processing pipeline that uses SMPL-X as a unified interface to process wrist and hand poses data, feeding into our Phantom System with joint-to-joint mapping and non-collision retargeting network; (3) Support for different robot platforms as output devices for executing the mapped movements.

tion mapping through the seamless integration of multiple components. Our system architecture utilizes IMU-based motion capture systems and mocap gloves to estimate wrist (Section III-A) and hand poses (Section III-B.1). We use the SMPL-X standard (Section III-A.1) to bridge all modules together, enabling flexible integration while maintaining system cohesion. These inputs are mapped to the robotic hand using our joint-to-joint retargeting approach (Section III-B.2) and non-collision retargeting module (Section III-C). We design each module to be independent yet interoperable, enabling flexible system configuration while maintaining robust performance.

We present the major contributions of TelePhantom to advance the field of teleoperation:

- **Low-Cost System:** We introduce an economical yet high-performance teleoperation system that integrates inertial motion capture technology and mocap gloves, with a total hardware cost under \$1,000, making it affordable for research.
- **Interactive Visual Assistance:** We develop a visualization interface that enables users to preview intended actions before execution, enhancing teleoperation precision and accessibility for both novice and experienced users during complex tasks.
- **Versatile Modules:** We design a modular assisted teleoperation pipeline that bridges various input devices with different robot end-effectors through joint-to-joint mapping and non-collision retargeting. This cross-platform design enables the versatile module to be integrated with diverse input methods and robots, making it a flexible solution for various manipulation scenarios.

II. RELATED WORK

A. Robot Teleoperation Frameworks for Manipulation

The growing interest in training robots via imitation learning has driven the need for extensive, high-quality real robot datasets. Teleoperation provides an efficient method for demonstrating and recording intricate robotic tasks. Researchers have explored various teleoperation systems, including VR controllers [1]–[3], motion capture [12]–[14], wearable gloves [11], [15]–[17], exoskeletons [18], [19], and other low-cost devices, each offering distinct benefits in terms of accessibility, precision, and generalizability.

While vision-based teleoperation methods offer a relatively low-cost solution [1]–[3], [6], they face significant challenges, including limited degrees of freedom (DoFs), constrained reachable workspace, and high computational demands. Although specialized hardware [4] can improve accuracy, it substantially increases system costs. Recent unified teleoperation frameworks attempt to address these limitations but often introduce new trade-offs. Many systems [3], [6] prioritize implementation simplicity by tracking only fingertip positions rather than enabling detailed joint-level control. Furthermore, their customization options typically require time-consuming manual parameter tuning that demands significant expertise.

B. Visual Feedback in Teleoperation Systems

Visual feedback plays a crucial role in teleoperation systems by providing users with spatial awareness and task-relevant information. Traditional approaches primarily rely on real-time camera feeds [20], [21], which can be limited by occlusions and restricted viewing angles. Moreover, the lack of preview capabilities for intended commands leaves users (especially novice users) uncertain about the robot’s response, which can increase error rates and user fatigue.

To address these limitations, researchers have explored enhanced visualization techniques [22]–[24] that overlay

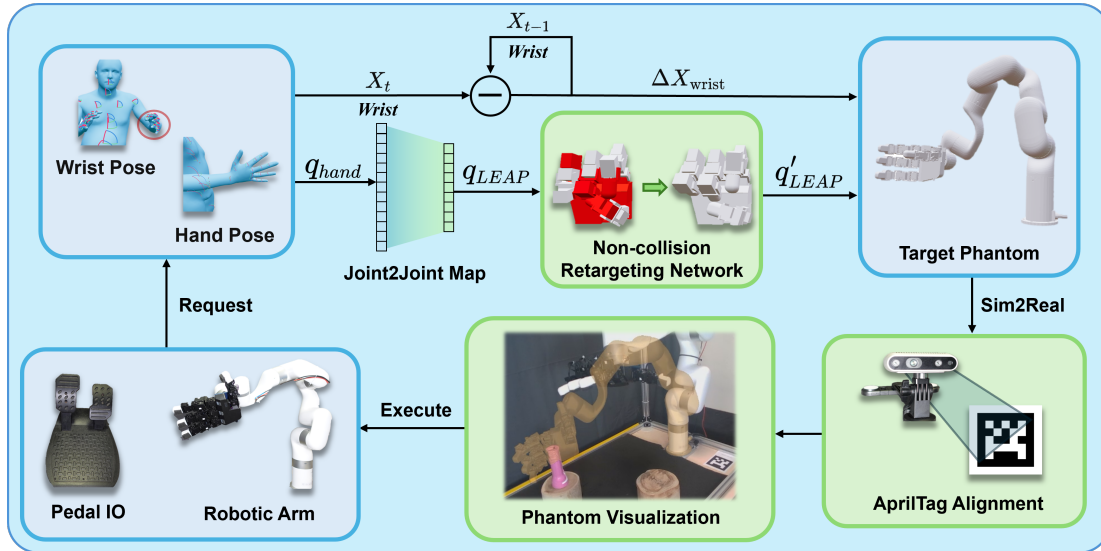


Fig. 3: **Pipeline of Our Assisted Module:** The system tracks user wrist and hand poses, maps them to robot joint configurations through joint-to-joint mapping and non-collision retargeting, and provides visual preview before physical execution. We achieve precise alignment between virtual and physical robots through AprilTag calibration.

virtual information onto the workspace view. While these approaches improve user perception by displaying planned trajectories and environmental constraints, they primarily focus on visualizing task-specific elements. This focus on task-specific visualization leaves users uncertain about how the robot will execute its commands.

III. MODULAR TELEOPERATION FRAMEWORK

Our teleoperation system consists of three main components: wrist pose estimation via IMU-based tracking, hand pose estimation using a motion capture glove, and non-collision retargeting for safe robot command generation. The following subsections detail each component of this pipeline.

A. Wrist Pose Estimation

1) *SMPL-X Standard:* We adopt the SMPL-X standard [25] as our unified human representation. The SMPL-X model represents a kinematic tree with standardized joint coordinate systems, where each joint’s pose describes a rotation and translation relative to its parent frame. This hierarchical structure enables consistent pose representation across different motion capture devices and simplifies the integration with our TelePhantom system.

2) *IMU-based Tracking System:* While many researchers adopt vision-based motion capture systems in teleoperation, these systems require multiple cameras, precise calibration, and controlled lighting conditions, which limits their practical deployment. IMU-based motion capture offers robust tracking regardless of visual conditions and occlusions.

Our system uses IMU sensors located on the user’s palm, forearm, and upper arm. Given the three IMUs, we utilize the REBOCAP framework [26] to obtain the specific SMPL-X model of the human body [25], [27]. Following the SMPL-X convention, we define the world frame system at the midpoint

between the feet. All positions and orientations in this paper are expressed in this coordinate system unless otherwise specified. After obtaining the SMPL-X model, we compute the wrist position $\mathbf{p}_w \in \mathbb{R}^3$ and orientation $\mathbf{R}_w \in SO(3)$ relative to this world frame.

Based on the wrist parameters, we map the user’s wrist pose to the end-effector pose through a transformation function \mathcal{T} . Specifically, we use the relative wrist position to control the end-effector position and the absolute wrist orientation to control the end-effector orientation:

$$\mathbf{p}_e(t) = \mathbf{p}_e(0) + (\mathbf{p}_w(t) - \mathbf{p}_w(0)), \quad \mathbf{R}_e(t) = \mathbf{R}_w(t), \quad (1)$$

where $\mathbf{p}_e(t)$ and $\mathbf{R}_e(t)$ represent the end-effector position and orientation at time t , and $\mathbf{p}_w(t)$ and $\mathbf{R}_w(t)$ represent the user’s wrist position and orientation at time t .

B. Hand Pose Estimation

1) *Human Hand Joint Value Acquisition:* Vision-based methods typically use deep learning models to predict 3D joint positions $\{p_i \in \mathbb{R}^3\}_{i=1}^N$ from RGB or RGB-D images. Due to the projective nature of imaging, vision-based systems struggle with self-occlusion, forcing researchers to infer joint positions from priors rather than direct observation. In contrast, mocap gloves [28] offer direct joint angle measurements $\{q_i\}_{i=1}^{27}$ using flex sensors despite their higher hardware cost. For our teleoperation scenario, we opt for the mocap-based approach to ensure robust hand tracking.

2) *Joint-to-Joint Mapping:* We propose a direct joint-to-joint mapping function $\mathcal{M} : \mathbb{R}^{27} \rightarrow \mathbb{R}^{16}$ that transforms mocap glove readings to LEAP hand [29] joint configurations. Let $q_g \in \mathbb{R}^{27}$ denote the glove joint values and $q_r \in \mathbb{R}^{16}$ denote the robot joint values. For each robot joint i , we define

a mapping:

$$q_r^i = f_i(q_g^{k_i}), \quad i \in 1, \dots, 16, \quad (2)$$

where k_i is the corresponding glove joint index for robot joint i which is manually picked, and f_i is a linear transformation:

$$f_i(x) = s_i(x - b_i)r_i. \quad (3)$$

Here, $s_i \in \mathbb{R}^+$ is a scaling factor that normalizes the joint ranges, $b_i \in \mathbb{R}$ is a bias term that aligns the neutral positions, and $r_i \in \{-1, 1\}$ is a direction indicator that ensures consistent joint rotations. This mapping guarantees:

$$\max q_g^{k_i} \Leftrightarrow \max q_r^i, \quad \min q_g^{k_i} \Leftrightarrow \min q_r^i, \quad (4)$$

Where q_g and q_r represent the joint angles of the glove and the Leap Hand, respectively, and max and min denote their upper and lower joint limits.

C. Non-Collision Retargeting Network

In robotic manipulation systems, ensuring non-collision during operation is crucial for both physical simulator accuracy and hardware safety. Self-collisions can lead to unstable behavior in simulators and, more critically, cause hardware damage in real-world deployments. This challenge is particularly significant for high-DoF systems like the LEAP hand [29], where collisions often occur due to differences in action spaces and imprecise retargeting. As shown in Fig.4, direct mapping from human hand postures to robotic hands using existing retargeting approaches like [6] can result in self-collisions, as demonstrated in Fig.4 (a). While traditional collision avoidance methods can achieve real-time performance for simpler end-effectors, they rely on optimization-based approaches that become computationally intensive for high-DoF configurations.

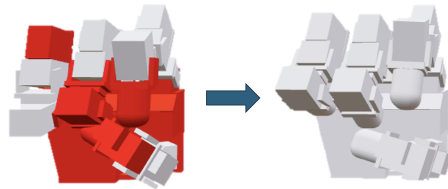
To address these challenges, we develop a learning-based framework with two key components: (1) a Self-Collision Prediction Network (CPN) that predicts collision probabilities for each joint configuration and (2) a Configuration Correction Network (CCN) that maps invalid configurations to their closest valid counterparts. The CCN is trained with a composite loss function that balances configuration similarity and collision avoidance, ensuring both motion continuity and physical feasibility. As demonstrated in Fig. 4 (b), our method successfully transforms problematic configurations into stable, safe positions while maintaining efficient real-time performance (about 60Hz). We provide the detailed technical implementation of this Pos-to-Pos Non-Collision Module in the Appendix.

IV. PHANTOM SYSTEM

The phantom system aims to provide safe and intuitive robot teleoperation through a phantom-based motion preview mechanism. The process consists of three key steps: (1) the user’s motion commands are first rendered on a phantom robot, (2) the phantom is precisely aligned with the real robot using AprilTag markers [30], and (3) upon user confirmation via a foot pedal, the validated motion is executed by the physical robot. This preview-then-execute workflow, as shown in



(a) Current retargeting method [6] causing collision.



(b) Our Self-collision Avoidance Retargeting.

Fig. 4: Comparison of hand configuration retargeting methods: (a) shows the direct mapping between human and robot hands leading to self-collision; (b) demonstrates our collision-aware retargeting approach that maintains safe configurations.

Fig. 3, enables users to verify and adjust planned motions before actual execution, significantly improving teleoperation safety and efficiency.

A. Why Phantom System Assistance?

1) *Current Challenges:* Traditional teleoperation approaches face significant challenges in data quality when collecting demonstrations for imitation learning. During complex manipulation tasks, users frequently make exploratory movements that contaminate the demonstration data with sub-optimal trajectories.

In our hanging insertion experiments, we observed that users using direct teleoperation required an average of 4 corrective movements per attempt. These adjustments typically involved probing movements to locate the socket edge and multiple approach angle refinements before successful insertion. Such trial-and-error behavior introduced significant noise into the collected datasets. This issue is particularly problematic for training imitation learning models, which benefit most from clean, purposeful demonstrations rather than trajectories cluttered with exploratory movements.

2) *Proposed Solution:* Our phantom-assisted teleoperation system addresses these data quality challenges through a novel preview mechanism. By visualizing a virtual “phantom” representation of the robot’s intended motion before executing physical movements, users can preview and refine their commands before committing to actual robot motion. This preview capability eliminates the need for exploratory movements in the physical space, as the real robot remains stationary until the user confirms the phantom pose. This design ensures that recorded trajectories contain only intentional, task-relevant actions without the noise of exploratory movements, directly benefiting downstream imitation learning applications with higher-quality demonstration data.

B. Technical Implementation of Phantom System

1) *Sim-to-Real Alignment Using AprilTag*: To maintain precise alignment between the phantom and physical robot across multiple camera viewpoints, we implement a robust calibration system using AprilTags [30]. Our approach establishes reliable reference frames through hand-eye calibration, and AprilTag pose estimation, linking both fixed and floating camera coordinate systems to the robot’s base frame.

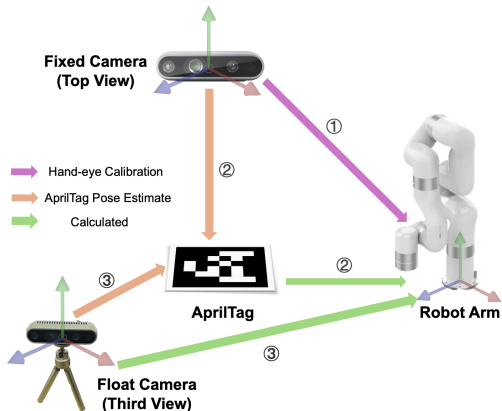
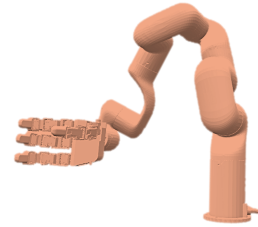


Fig. 5: **Our transformation relationship**: The number in the circle denotes the order of transformation acquisition.

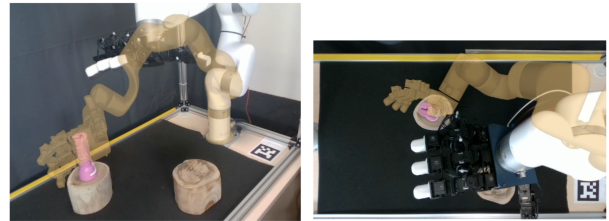
As shown in Fig. 5, our calibration procedure involves multiple sequential transformations. We begin with hand-eye calibration of the fixed top-view camera (1), followed by detecting the AprilTag’s pose from this camera’s perspective (2). Using these relationships, we can compute the transformation between the AprilTag and the robot base frame (2). For the additional floating third-view camera, we first detect the AprilTag pose from its viewpoint (3), which then allows us to establish its position relative to the robot base frame through the standard AprilTag reference (3). This chain of transformations ensures consistent phantom visualization regardless of camera movement or viewpoint changes, making our system robust for dynamic viewing scenarios.

2) *Robot Phantom Visualization*: Building upon this spatial alignment system, we implement the visual component of our phantom system. As shown in Fig. 6a, we use the pyrender [31] library to render the virtual robot through the previous float camera. The rendered phantom image is then composited with the actual camera feed using alpha blending, creating a seamless overlay where the virtual robot appears naturally integrated with the physical environment. This visualization approach requires careful calibration of the virtual camera parameters to match the physical cameras, ensuring that the phantom accurately reflects the robot’s intended configuration in the workspace. The resulting overlay provides users with an intuitive preview of planned motions.

3) *Multi-view Phantom Visualization*: Our phantom system supports multiple viewpoints to enhance spatial awareness during complex manipulation tasks. As shown in Fig. 6b and Fig. 6c, we deploy cameras to capture both third-person and top-down views of the workspace, allowing



(a) Real-time phantom rendering



(b) Third-person view

(c) Top-down view

Fig. 6: Rendering and Multi-view visualization system.

users to verify planned movements from complementary perspectives. For instance, during manipulation tasks, users can simultaneously monitor the robot’s vertical position from the third-person view while checking its planar alignment from the top-down view.

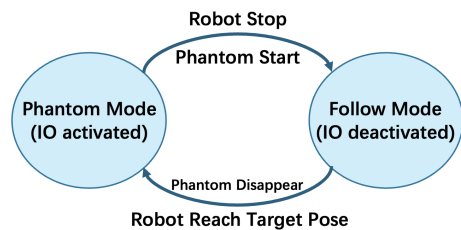


Fig. 7: State transition of phantom control

4) *IO Control for Phantom Visualization*: Our system uses a foot pedal as an intuitive control interface for state transitions. As shown in Fig. 7, when the IO is activated, the physical robot stops while the phantom appears and responds to user commands for motion preview. Upon IO deactivation, the phantom disappears, and the system extracts its final configuration as the target pose, bypassing any exploratory movements made during the preview. This target is then processed by the mplib motion planning library [33] to generate an optimal trajectory for execution. After reaching the target pose, the robot automatically resumes real-time teleoperation until the next IO is activated. This workflow ensures users execute only refined, intentional movements, eliminating exploratory motions from demonstration data.

V. EXPERIMENTS

Our experiments aim to address the following questions:

- (Q1) How effective is TelePhantom vs Baselines?
- (Q2) How beneficial is TelePhantom for new users?
- (Q3) How versatile is TelePhantom on robots?

Task	TelePhantom	Open Teach [3]	AnyTeleop [6]	Telekinesis [32]
Pick & Place	1.0	0.8	1.0	0.9
Hang	0.9	-	-	-
Pour	1.0	0.8	0.7	0.7
Box Rotation	1.0	-	0.6	0.6
Cup Stacking	1.0	-	0.7	0.3

TABLE I: **Real Robot Teleoperation Results.** For the baseline methods, we use success rate as a metric reported in their papers. Especially, we use the success rate of an expert as a metric for Open Teach [3].

Task	Success Rate			Average Success Execution Time (s)		
	w/o phantom	w/ phantom	Difference \uparrow	w/o phantom	w/ phantom	Difference \downarrow
Pick & Place	0.6	1.0	+0.4	23.56	13.55	-10.01
Hang	0.6	1.0	+0.4	29.30	30.83	+1.53
Pour	0.9	0.8	-0.1	43.20	36.13	-7.07
Box Rotation	0.6	0.8	+0.2	30.47	19.12	-11.35
Cup Stacking	0.5	1.0	+0.5	31.54	18.91	-12.63

TABLE II: Effect of Phantom Assistance on New User Performance.

A. Experiment Setup

TelePhantom integrates several key components. The user’s movements are captured via an inertial motion capture suit and a pair of strain gauge-based mocap gloves, providing high-fidelity joint angle data for both body posture and delicate hand movements. To visualize robot action before execution, we employ a RealSense RGB-D camera and render the phantom either on a standard 2D display or within a VR headset (e.g., Meta Quest 3). For the physical hardware, we use a UFactory xArm-6 robotic arm outfitted with a Leap hand [29], utilizing AprilTag [30] to align the initial poses of the phantom and the real robot.

Following the methodology outlined in [6], [32], users attempted each task 10 times. We reference the baseline success rates from their papers.

B. Real Robot Teleoperation

We test TelePhantom on five real-world tasks that highlight different manipulation challenges:

- **Pick & Place:** Grasp an object and place it at precise locations.
- **Pour:** Tilt and rotate a cup to pour the beans into another container.
- **Hang:** Hang a spoon on a peg, requiring both fine positioning and subtle wrist rotations.
- **Box Rotation:** Rotate a box to change its orientation.
- **Cup Stacking:** Stack a cup onto another cup.

Performance Comparison with Baselines. Addressing Q1 (effectiveness vs. baselines), we compare the real robot teleoperation performance of TelePhantom, operated by an expert, with Telekinesis [32], AnyTeleop [6] and Open Teach [3]. As summarized in Table I, TelePhantom outperforms baseline methods in terms of success rate. The baseline

methods are limited to simple, short-horizon tasks. While the baseline methods can handle basic tasks, they fail to accurately capture subtle wrist rotations and movements in more delicate operations like the hung task. The superior performance of TelePhantom in these scenarios demonstrates its capability to handle more challenging tasks effectively.

Effect of Phantom. To address Q2 (benefits for new users), we assess TelePhantom’s utility by measuring both the success rate and the average execution time on the real robot (demonstration time in imitation learning) with and without phantom. As shown in Table II, TelePhantom significantly improves the performance of new users by improving their task success rate. The execution time on a real robot corresponds to the demonstration time required for imitation learning. High-quality demonstrations are typically associated with shorter execution times. With the assistance of TelePhantom, new users achieve a lower average execution time, indicating that they can produce higher-quality demonstrations compared to users without access to TelePhantom. For new users, command visualization and reduced execution time not only decrease physical strain but also improve safety.

C. Deployment on Various Robots

TelePhantom’s modular design enables seamless adaptation to different input devices and end-effectors. Thanks to our robot-centric phantom approach and standardized transformation framework, users can readily configure the system for various robotic platforms by simply updating the kinematic parameters and transformation chain. This adaptability across different robot configurations, as posed in Q3, demonstrates TelePhantom’s versatility as a flexible teleoperation solution that can serve diverse robotic applications with minimal modification requirements.

VI. CONCLUSION

In this paper, we presented TelePhantom, a low-cost teleoperation system featuring AR phantom feedback designed for deployment across diverse robotic platforms. Our experiments demonstrate that TelePhantom offers sufficient flexibility and safety to successfully perform a variety of fine-grained tasks. Through its innovative phantom visualization approach, the system provides immediate, robot-centric feedback that enables users to preview and refine their commands before physical execution.

While our results show promising advances in teleoperation interfaces, a key limitation is the visual ambiguity caused by occlusions between the phantom and scene objects. Future work could address this by incorporating depth information from RGB-D cameras to create more accurate spatial relationships between virtual and physical elements.

Addressing these visualization challenges could yield several essential benefits. Improved occlusion handling would reduce user uncertainty during complex manipulation tasks, leading to higher-quality demonstration data for imitation learning. Additionally, more accurate spatial rendering would create a more intuitive teleoperation experience, potentially reducing user training time and cognitive load. These improvements would further advance TelePhantom's goal of providing accessible, effective teleoperation capabilities across diverse robotic applications.

REFERENCES

- [1] X. Cheng, J. Li, S. Yang, G. Yang, and X. Wang, "Open-television: Teleoperation with immersive active visual feedback," *arXiv preprint arXiv:2407.01512*, 2024.
- [2] R. Ding, Y. Qin, J. Zhu, C. Jia, S. Yang, R. Yang, X. Qi, and X. Wang, "Bunny-visionpro: Real-time bimanual dexterous teleoperation for imitation learning," *arXiv preprint arXiv:2407.03162*, 2024.
- [3] A. Iyer, Z. Peng, Y. Dai, I. Guzey, S. Haldar, S. Chintala, and L. Pinto, "Open teach: A versatile teleoperation system for robotic manipulation," *arXiv preprint arXiv:2403.07870*, 2024.
- [4] Z. Fu, T. Z. Zhao, and C. Finn, "Mobile aloha: Learning bimanual mobile manipulation with low-cost whole-body teleoperation," *arXiv preprint arXiv:2401.02117*, 2024.
- [5] A. George, A. Bartsch, and A. B. Farimani, "Openvr: Teleoperation for manipulation," *arXiv preprint arXiv:2305.09765*, 2023.
- [6] Y. Qin, W. Yang, B. Huang, K. Van Wyk, H. Su, X. Wang, Y.-W. Chao, and D. Fox, "Anyteleop: A general vision-based dexterous robot arm-hand teleoperation system," *arXiv preprint arXiv:2307.04577*, 2023.
- [7] G. Zhu, X. Xiao, C. Li, J. Ma, G. Ponraj, A. Prituja, and H. Ren, "A bimanual robotic teleoperation architecture with anthropomorphic hybrid grippers for unstructured manipulation tasks," *Applied Sciences*, vol. 10, no. 6, p. 2086, 2020.
- [8] D. Leonardis, M. Gabardi, S. Marcheschi, M. Barsotti, F. Porcini, D. Chiaradia, and A. Frisoli, "Hand teleoperation with combined kinaesthetic and tactile feedback: A full upper limb exoskeleton interface enhanced by tactile linear actuators," *Robotics*, vol. 13, no. 8, p. 119, 2024.
- [9] K. Shaw, Y. Li, J. Yang, M. K. Srirama, R. Liu, H. Xiong, R. Mendonca, and D. Pathak, "Bimanual dexterity for complex tasks," *arXiv preprint arXiv:2411.13677*, 2024.
- [10] Y. Park and P. Agrawal, "Using apple vision pro to train and control robots," 2024.
- [11] C. Wang, H. Shi, W. Wang, R. Zhang, L. Fei-Fei, and C. K. Liu, "Dexcap: Scalable and portable mocap data collection system for dexterous manipulation," *arXiv preprint arXiv:2403.07788*, 2024.
- [12] M. Hirschmanner, C. Tsiourti, T. Patten, and M. Vincze, "Virtual reality teleoperation of a humanoid robot using markerless human upper body pose imitation," in *2019 IEEE-RAS 19th International Conference on Humanoid Robots (Humanoids)*, 2019, pp. 259–265.
- [13] C. Stanton, A. Bogdanovych, and E. Ratanasena, "Teleoperation of a humanoid robot using full-body motion capture, example movements, and machine learning," in *Proc. Australasian Conference on Robotics and Automation*, vol. 8, 2012, p. 51.
- [14] N. Miller, O. C. Jenkins, M. Kallmann, and M. J. Mataric, "Motion capture from inertial sensing for untethered humanoid teleoperation," in *4th IEEE/RAS International Conference on Humanoid Robots, 2004.*, vol. 2. IEEE, 2004, pp. 547–565.
- [15] H. Liu, Z. Zhang, X. Xie, Y. Zhu, Y. Liu, Y. Wang, and S.-C. Zhu, "High-fidelity grasping in virtual reality using a glove-based system," in *2019 international conference on robotics and automation (icra)*. IEEE, 2019, pp. 5180–5186.
- [16] M. Mosbach, K. Moraw, and S. Behnke, "Accelerating interactive human-like manipulation learning with gpu-based simulation and high-quality demonstrations," in *2022 IEEE-RAS 21st International Conference on Humanoid Robots (Humanoids)*. IEEE, 2022, pp. 435–441.
- [17] M. Schwarz, C. Lenz, A. Rochow, M. Schreiber, and S. Behnke, "Nimbro avatar: Interactive immersive telepresence with force-feedback telemanipulation," in *2021 IEEE/RSJ International Conference on Intelligent Robots and Systems (IROS)*. IEEE, 2021, pp. 5312–5319.
- [18] S. Yang, M. Liu, Y. Qin, R. Ding, J. Li, X. Cheng, R. Yang, S. Yi, and X. Wang, "Ace: A cross-platform visual-exoskeletons system for low-cost dexterous teleoperation," *arXiv preprint arXiv:2408.11805*, 2024.
- [19] P. Wu, Y. Shentu, Z. Yi, X. Lin, and P. Abbeel, "Gello: A general, low-cost, and intuitive teleoperation framework for robot manipulators," 2023.
- [20] D. A. Lawrence, "Stability and transparency in bilateral teleoperation," *IEEE transactions on robotics and automation*, vol. 9, no. 5, pp. 624–637, 1993.
- [21] A. M. Ousaid, D. S. Haliyo, S. Régnier, and V. Hayward, "A stable and transparent microscale force feedback teleoperation system," *IEEE/ASME Transactions on Mechatronics*, vol. 20, no. 5, pp. 2593–2603, 2015.
- [22] Z. Zhao, P. Huang, Z. Lu, and Z. Liu, "Augmented reality for enhancing tele-robotic system with force feedback," *Robotics and Autonomous Systems*, vol. 96, pp. 93–101, 2017.
- [23] D. Lee and Y. S. Park, "Implementation of augmented teleoperation system based on robot operating system (ros)," in *2018 IEEE/RSJ International Conference on Intelligent Robots and Systems (IROS)*. IEEE, 2018, pp. 5497–5502.
- [24] P. Milgram, A. Rastogi, and J. J. Grodski, "Telerobotic control using augmented reality," in *Proceedings 4th IEEE International Workshop on Robot and Human Communication*. IEEE, 1995, pp. 21–29.
- [25] G. Pavlakos, V. Choutas, N. Ghorbani, T. Bolkart, A. A. Osman, D. Tzionas, and M. J. Black, "Expressive body capture: 3d hands, face, and body from a single image," in *Proceedings of the IEEE/CVF conference on computer vision and pattern recognition*, 2019, pp. 10975–10985.
- [26] D. Technology, "Rebocap: Affordable imu-based motion capture system," <http://rebocap.com/>, 2024, a 15-point full-body IMU motion capture system for games, films, animations, human motion analysis and live streaming applications. Accessed: 2024-03-16.
- [27] J. Romero, D. Tzionas, and M. J. Black, "Embodied hands: Modeling and capturing hands and bodies together," *ACM Transactions on Graphics, (Proc. SIGGRAPH Asia)*, vol. 36, no. 6, Nov. 2017.
- [28] UdexReal, "UdCap: Silk-like VR gloves for SteamVR," Kickstarter Campaign, 2024, available at: <https://www.kickstarter.com/projects/udexreal/udcap-silk-like-vr-gloves-for-steamvr>.
- [29] K. Shaw, A. Agarwal, and D. Pathak, "Leap hand: Low-cost, efficient, and anthropomorphic hand for robot learning," *Robotics: Science and Systems (RSS)*, 2023.
- [30] E. Olson, "Apriltag: A robust and flexible visual fiducial system," in *2011 IEEE international conference on robotics and automation*. IEEE, 2011, pp. 3400–3407.
- [31] M. Matl, "Pyrender," <https://github.com/mmatl/pyrender>, 2019.
- [32] A. Sivakumar, K. Shaw, and D. Pathak, "Robotic telekinesis: Learning a robotic hand imitator by watching humans on youtube," *arXiv preprint arXiv:2202.10448*, 2022.
- [33] H. S. Lab, "Mplib: A motion planning library," <https://github.com/haosulab/mplib>, 2023, accessed: 2024-12-15.

A. Technical Implementation of Pos-to-Pos Non-Collision Module

Due to differences in action space and limitations in the precision of the retargeting algorithm, the configuration of a dexterous robotic hand often generates invalid self-collision configurations. These invalid configurations not only lack operational utility but also risk system failure or hardware damage. To address this issue, we propose a method for mapping invalid configurations to their closest valid counterparts, enabling recovery from self-collision scenarios.

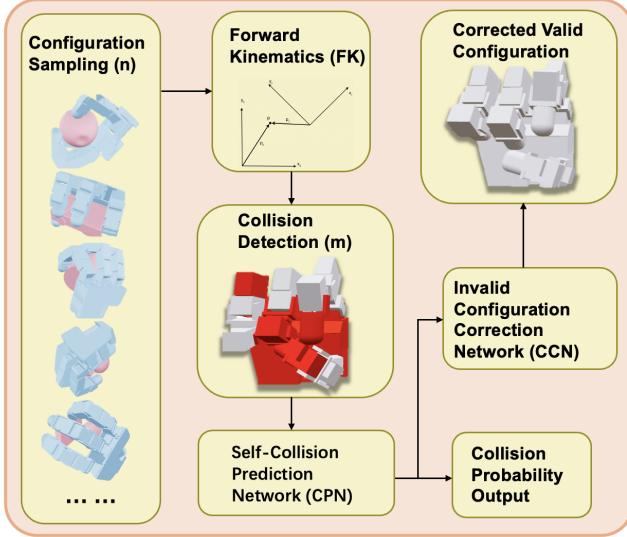


Fig. 8: Pipeline of the Non-collision Module

Fig. 8 illustrates our pos2pos implementation pipeline, which consists of several interconnected components for handling robot hand configurations.

1) *Self-Collision Prediction Network (CPN)*: To facilitate the transformation from invalid to valid configurations, we first develop a **Self-Collision Prediction Network (CPN)**. The primary objective of CPN is to predict the likelihood of self-collision for each link within a given joint configuration.

The training dataset is generated by uniformly sampling n configurations from the robot’s action space. For each sampled configuration, the system employs forward kinematics (FK) to compute the robot’s pose. A collision detection algorithm (e.g., geometric or physics-based) then checks the pose to derive m collision labels for the links. Each label indicates whether a link is in a collision state.

The CPN takes joint configurations as input and outputs collision probabilities for all joints. We train the network using the binary cross-entropy (BCE) loss function, defined as:

$$L_{\text{CPN}} = \frac{1}{m} \sum_{i=1}^m \text{BCE}(p_i, t_i), \quad (5)$$

where p_i and t_i represent the predicted and true collision probabilities, respectively.

2) Invalid Configuration Correction Network (CCN):

Building on the CPN, we introduce an **Invalid Configuration Correction Network (CCN)** to map invalid configurations to valid ones. The CCN takes an invalid configuration as input and outputs a corrected configuration that minimizes collision risks while closely resembling the original input.

The CCN training process minimizes a composite loss function comprising two components:

- **Mean Squared Error (MSE) Loss**: Ensures the corrected configuration closely resembles the original configuration.

$$L_{\text{MSE}} = \frac{1}{n} \sum_{i=1}^n (\hat{q}_i - q_i)^2, \quad (6)$$

where q_i and \hat{q}_i denote the original and corrected joint configurations, respectively.

- **Collision Probability Loss**: Leverages the CPN to compute the mean collision probability of the corrected configuration and aims to minimize this value.

$$L_{\text{Collision}} = \frac{1}{m} \sum_{i=1}^m p_i(\hat{q}), \quad (7)$$

where $p_i(\hat{q})$ represents the collision probability of joint i in the corrected configuration \hat{q} .

We define the total loss function as:

$$L = \alpha L_{\text{MSE}} + \beta L_{\text{Collision}}, \quad (8)$$

where α and β are hyperparameters balancing the two loss components.

3) *Explanation and Optimization Strategy*: The loss terms in the proposed framework serve distinct roles:

- L_{MSE} ensures the corrected configuration retains continuity with the original input.
- $L_{\text{Collision}}$ minimizes the likelihood of self-collision in the corrected configuration.
- The hyperparameters α and β significantly influence the training outcomes, and we optimize their values through grid search.

The CCN employs a fully connected multi-layer perceptron (MLP) architecture. The input is the invalid joint configuration q , and the output is the corrected configuration \hat{q} . We train the model using the Adam optimizer with a learning rate η and monitor convergence via the collision rate on a validation dataset.

4) *Summary*: By integrating the CPN and CCN, we efficiently transform invalid self-collision configurations into valid ones. This approach ensures the validity and continuity of robotic configurations, laying a robust foundation for subsequent task execution.

B. Visualization of our tasks

We visualize the execution process of our five manipulation tasks in Figure 9-13. They demonstrate the execution sequences of five manipulation tasks: picking and placing a cup, hanging a spoon on a peg, pouring beans between containers, rotating a box, and stacking cups.

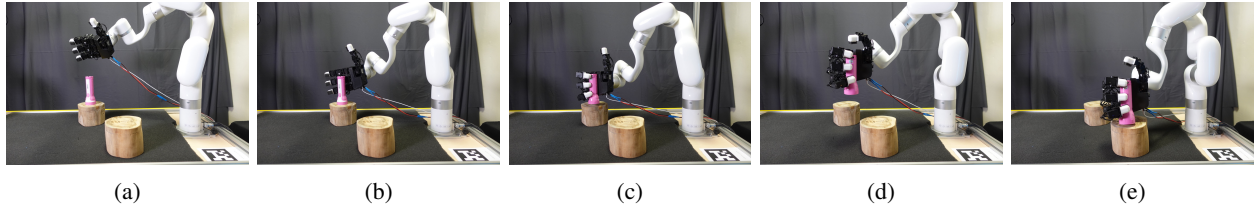


Fig. 9: Pick&Place Visualization

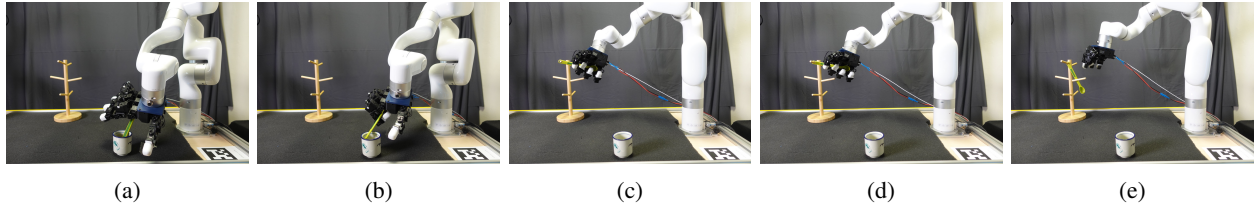


Fig. 10: Hang Visualization

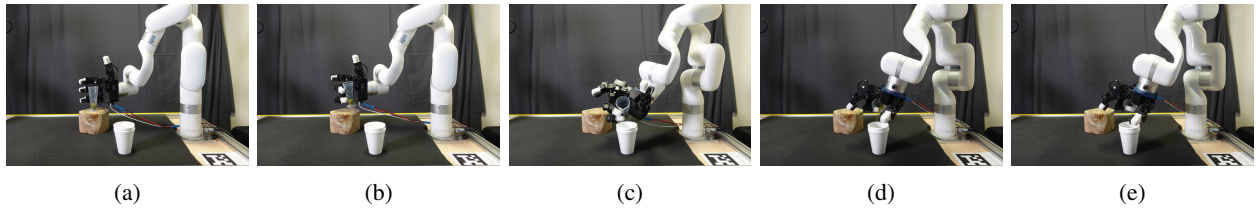


Fig. 11: Pour Visualization

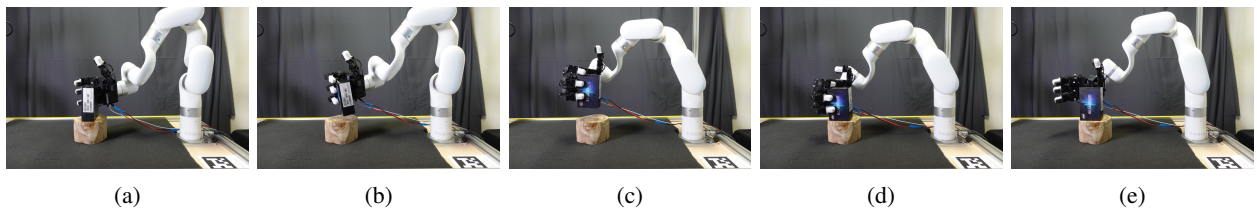


Fig. 12: Box Rotation Visualization

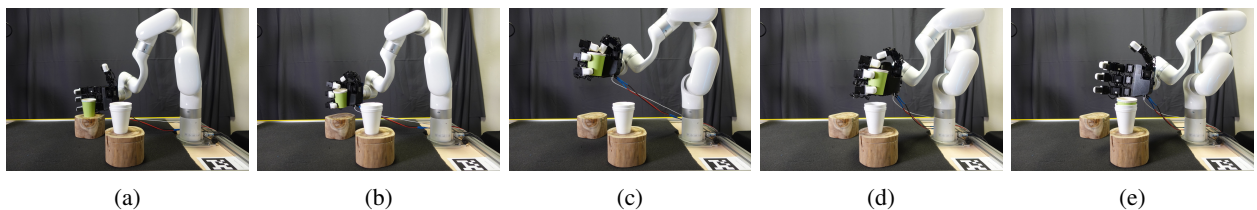


Fig. 13: Cupstack Visualization